

**UCSF**

**UC San Francisco Electronic Theses and Dissertations**

**Title**

Measuring mTORC1 Signaling with Non-Invasive (89)Zr-Transferrin PET

**Permalink**

<https://escholarship.org/uc/item/5rj4p3mh>

**Author**

Hsiao, Jeffrey Chieh

**Publication Date**

2018

Peer reviewed|Thesis/dissertation

Measuring mTORC1 Signaling with  
Non-Invasive (89)Zr-Transferrin PET

by

Jeffrey Chieh Hsiao

THESIS

Submitted in partial satisfaction of the requirements for the degree of

MASTER OF SCIENCE

in

Biomedical Imaging

in the

GRADUATE DIVISION



*My thesis is dedicated to my family  
and to anyone who may find it  
interesting and/or informative*

## Acknowledgments

I would like to first acknowledge the members of the Evans lab: Michael J. Evans<sup>1,5,6,\*</sup>, Anna Moroz<sup>1,2</sup>, Charles Truillet<sup>1</sup>, Junnian Wei<sup>1</sup>, Yung-Hua Wang<sup>1</sup> for their generous supervision and mentorship. I would also like to acknowledge the collaborators on this project: Sean D. Carlin<sup>3</sup>, Davide Ruggero<sup>4,5</sup>, Kevin Leung<sup>6</sup>, James A. Wells<sup>6</sup>, Hilaire Lam<sup>7</sup>, and Elizabeth P. Henske<sup>7</sup> for their contributions. Next, I would like to thank my committee members: David Wilson, Robert Flavell, and Henry VanBrocklin for their guidance and feedback. Lastly, it is my pleasure to acknowledge the administration of the UCSF MSBI program: Alastair Martin, David Saloner, Rukayah Abdolcader, and Susan Noworolski for their unwavering support. Thank you.

<sup>1</sup>Department of Radiology and Biomedical Imaging, University of California San Francisco, 505 Parnassus Ave, San Francisco CA 94143

<sup>2</sup>Skolkovo Institute of Science and Technology, Skolkovo Innovation Center, 3 Nobel St, Moscow, Russia, 143026

<sup>3</sup>Department of Radiology, Hospital of the University of Pennsylvania, 3400 Spruce Street, Philadelphia, PA 19104

<sup>4</sup>Department of Urology, <sup>5</sup>Helen Diller Family Comprehensive Cancer Center, <sup>6</sup>Department of Pharmaceutical Chemistry, University of California San Francisco, 505 Parnassus Ave, San Francisco CA 94143

<sup>7</sup>Center for LAM Research and Clinical Care, Brigham and Women's Hospital, Harvard Medical School, 45 Francis Street, Boston, MA 02115

# Measuring mTORC1 Signaling with Non-Invasive $^{89}\text{Zr}$ -Transferrin PET

Jeffrey Chieh Hsiao

The diagnosis and management of the phenotypically heterogeneous and progressive disorders tuberous sclerosis complex (TSC) and lymphangiomyomatosis (LAM) is a significant clinical challenge owing to a lack of disease specific biomarkers. Because the genetic mutations in TSC1 and/or TSC2 characteristic of TSC and LAM activate mTORC1 signaling, we hypothesized that disease burden could be measured with PET using  $^{89}\text{Zr}$ -transferrin (Tf). Toward this goal, we show that spontaneous renal cystadenomas arising in a genetically engineered mouse model heterozygous for *Tsc2* were readily detectable with  $^{89}\text{Zr}$ -Tf PET. Moreover, subcutaneous implants of TSC and LAM cell line models consistently harbored high avidity for  $^{89}\text{Zr}$ -Tf in vivo. Deeper mechanistic studies showed that transferrin receptor expression and Tf biology were mTORC1 regulated in TSC and LAM models. Finally, the early treatment effects of clinically approved and experimental systemic therapies for TSC and LAM were interpretable using  $^{89}\text{Zr}$ -Tf PET. In summary, these data advance a translatable molecular imaging strategy that may be capable of detecting and longitudinally monitoring whole body TSC and LAM disease burden.

## Table of Contents:

<u>Introduction</u>	<u>1</u>
<u>Results</u>	<u>2</u>
<u>Discussion</u>	<u>4</u>
<u>Methods</u>	<u>5</u>
<u>Figures</u>	<u>10</u>
<u>References</u>	<u>14</u>

List of Figures:

Figure 1	10
Figure 2	11
Figure 3	13



## Introduction:

Tuberous sclerosis complex (TSC) is an autosomal dominant disease predicated on genetic mutations that inactivate the TSC1/TSC2 complex (Crino, 2006; Henske, 2016). TSC is generally a non-malignant, but progressive disorder that manifests as a bloom of hamartomas in various organs from infancy into adulthood, many of which will incur debilitating symptoms (e.g. epilepsy, impaired cognitive development). TSC also significantly elevates the risk of secondary disorders that arise in part due to TSC1/2 inactivation, including the destructive lung disease lymphangioleiomyomatosis (LAM) (Henske, 2012).

The clinical courses of TSC and LAM are highly unpredictable. On this basis, non-invasive biomarkers of disease burden and/or activity are crucial for effective disease management. For instance, routine electroencephalogram in asymptomatic TSC infants captures those at high risk for developing epilepsy, which in turn motivates prophylactic treatment with vigabatrin for seizure control (Wu, 2016). Moreover, elevated serum VEGF-D levels in women with TSC can signal the onset of LAM, which, when combined with high resolution CT, enables earlier diagnosis and treatment (Nijmeh, 2018). Despite these milestones, the overwhelming majority of clinical manifestations of TSC and LAM have no cognate biomarker for diagnosis, predicting aggressive versus indolent disease, or monitoring response to systemic therapies.

Although TSC and LAM are phenotypically heterogeneous, a unifying subcellular consequence of TSC1/2 loss is elevated mTORC1 signaling, regardless of how and in what organs clinically problematic cells manifest (Huang, 2008). On this basis, we hypothesized that a molecular event regulated downstream of mTORC1 could serve as

a useful biomarker of disease burden. mTORC1 regulates a broad spectrum of metabolic changes, including transferrin dependent Fe(III) uptake into cells (Galvez, 2007; Abe, 2008). We recently demonstrated that radiolabeled transferrin can be used to non-invasively measure mTORC1 activity in models of malignant cancers using PET (Truillet, 2017). Therefore, the goal of this study was to determine if non-malignant models representative of TSC and LAM are detectable with <sup>89</sup>Zr-transferrin.

## Results:

We first tested if spontaneous growths arising in a genetically engineered mouse (GEM) model of TSC were detectable with <sup>89</sup>Zr-Tf PET. The A/J GEM model bears germline deletion of one *Tsc2* allele, and mice predominantly develop renal cystadenomas within one year after birth (Onda, 1999). Eight-month-old male A/J mice were treated with <sup>89</sup>Zr-Tf, and the biodistribution of the radiotracer was studied at 48 hours post injection. Focal accumulation of the radiotracer within small regions of the transgenic kidneys was visually obvious on PET/CT (**Figure 1A**). Moreover, PET/CT of the surgically excised transgenic kidneys revealed numerous regions of high radiotracer uptake compared to wild type kidneys (**Figure 1B**). Digital autoradiography was performed to identify the source of the radioactivity, and the regions of highest radiotracer accumulation co-localized with renal cystadenomas identified by H&E (**Figure 1C**).

We next performed in vivo studies to determine if *Tsc2* mutant tumors are avid for <sup>89</sup>Zr-Tf on PET. <sup>89</sup>Zr-Tf uptake was evaluated over time in intact female mice bearing subcutaneous ELT3 (rat LAM) tumors, and tumors were clearly detectable on

the flank of mice within 8 hours post i.v. injection of  $^{89}\text{Zr-Tf}$  (**Figure 2A**). Moreover, serial imaging showed increasing retention of  $^{89}\text{Zr-Tf}$  in the tumors from 8 – 48 hours. Ex vivo biodistribution studies corroborated the PET findings, as tumor uptake of  $^{89}\text{Zr-Tf}$  rose from 8 - 72 hours post injection. A separate cohort of intact male mice bearing subcutaneous *tsc2* *ang1* (mouse angiomyolipoma) tumors were treated with  $^{89}\text{Zr-Tf}$ , and radiotracer biodistribution was studied over time. As with the ELT3 cohort, xenografts were visualized within a day post injection, with peak radiotracer uptake in the tumor occurring between 24 – 48 hours post injection (**Figure 2B**). Lastly, we conducted a broader survey of  $^{89}\text{Zr-Tf}$  uptake at 48 hours post injection in mice bearing *Tsc2* mutant tumor models 105K (mouse angiomyolipoma), 621-101 (human LAM), and *Tsc1* null human bladder cancer cell lines, 97-1 and RT4.  $^{89}\text{Zr-Tf}$  uptake was detected in all tumors at levels above background (**Figure 2C**).

To test if TFRC protein is upregulated in TSC models in an mTORC1-dependent fashion, we applied flow cytometry to ELT3 V3 and T3, isogenic pairs stably expressing an empty vector and a vector with a wild type *Tsc2* insert, respectively (Li, 2014). TFRC levels were ~40% higher in ELT3 V3 compared to ELT3 T3, suggesting that restoration of wild type levels of the TSC1/TSC2 complex reduces TFRC expression (**Figure 3A**). Next, cellular uptake of Tf was inhibited in vitro in the panel of cell lines with endogenous *Tsc1* or *Tsc2* mutations due to treatment with mTOR inhibitors (**Figure 3B**). Importantly, treatment with a bioactive dose of doxorubicin did not impact Tf uptake, underscoring its dependence on mTOR activity, and not simply associated with suppression of cellular proliferation and survival. Collectively, these data underscore that TFRC expression and Tf uptake is mTORC1 regulated in TSC and LAM

cell lines.

To determine if treatment induced changes in intracellular mTORC1 signaling are sufficiently large to be quantified with  $^{89}\text{Zr}$ -Tf PET, mice bearing subcutaneous *tsc2* *ang1* tumors were treated once daily via gavage for 5 days with RAD001 (10 mg/kg), BEZ235 (30 mg/kg), doxorubicin (5 mg/kg), or vehicle. Animals received  $^{89}\text{Zr}$ -Tf intravenously on day 3, and PET and biodistribution studies were conducted 48 hours after radiotracer injection. Treatment with mTOR inhibitors significantly reduced tumor uptake of  $^{89}\text{Zr}$ -Tf uptake compared to vehicle and doxorubicin treatment (**Figure 3C** and **3D**), suggesting that  $^{89}\text{Zr}$ -Tf PET can measure treatment induced changes in mTORC1 signaling non-invasively.

## Discussion:

We describe herein a new molecular imaging approach that may improve the detection and monitoring of clinically problematic cells arising from TSC and/or LAM. Our strategy exploits a functional connection between loss of TSC1/2, and an mTORC1 dependent increase in cell surface TfRC expression and Tf uptake into cells. Importantly,  $^{89}\text{Zr}$ -Tf detected renal cystadenomas spontaneously arising in a GEM model of TSC. Moreover, a pathologically diverse panel of TSC and LAM cell lines all bore high avidity for Tf in an mTORC1 dependent fashion. Lastly, short term treatment of TSC and LAM xenografts with mechanistically discrete mTORC1 inhibitors showed that intracellular changes in mTORC1 signaling can be measured with  $^{89}\text{Zr}$ -Tf PET prior to the onset of volumetric regression.

The limited clinical data suggest that conventional PET/CT is not useful for

studying benign disease burden, as angiomyolipoma and LAM are not avid for  $^{18}\text{F}$ -fluorodeoxyglucose (FDG) (Pandit, 2001; Young, 2009; Lin, 2013). Malignant angiomyolipoma is detectable with  $^{18}\text{F}$ -FDG and  $^{11}\text{C}$ -acetate PET; however, the overall risk of developing malignancies due to TSC or LAM is minimal (Griffin, 2017; Arnold, 2009; Ho, 2010; Lhommel, 2005).  $^{11}\text{C}$ - $\alpha$ -methyl-L-tryptophan PET may be useful for the detection of epileptogenic brain tubers (Chugani, 2013; Fedi, 2003), though its mechanism of action makes it is unlikely that this radiotracer will be useful for detecting disease outside of the brain.

While  $^{89}\text{Zr}$ -Tf is experimental and not human ready, we have performed PET studies with  $^{68}\text{Ga}$ -citrate, which potently binds to apo-Tf after i.v. administration (Larson, 1978). In preclinical tumor models,  $^{68}\text{Ga}$ -citrate has a virtually identical biodistribution to  $^{89}\text{Zr}$ -Tf, despite a significantly shorter uptake time (4 versus 48 hours) (Aggarwal, 2017). Moreover, we have conducted  $^{68}\text{Ga}$ -citrate PET/CT and PET/MR studies in over 20 patients with castration resistant prostate cancer and hepatocellular carcinoma at UCSF since 2015 (Aggarwal, 2017; Behr, 2016; Mari Aparici, 2017). That  $^{68}\text{Ga}$ -citrate is avidly taken up by these tumor types, known to have mTORC1 hyperactivity, gives us optimism that the encouraging preclinical data with  $^{89}\text{Zr}$ -Tf will translate into meaningful clinical findings for TSC and LAM patients when imaged with  $^{68}\text{Ga}$ -citrate PET. We are currently pursuing proof-of-concept clinical imaging studies to this end.

## Methods:

**General Methods:** RT4, tsc2 ang1 and HCV29 cells were acquired from ATCC and

subcultured according to manufacturer's recommendations. 97-1 human bladder cancer cell line was kindly provided by Dr. Margaret A. Knowles University of Leeds, UK and subcultured in F12 media Kaighn's modification (HyClone™, Logan, Utah) with 10% (v/v) fetal calf serum (FCS), 1% penicillin/streptomycin (Pen/Strep). ELT3, 105K were subcultured in DMEM (Corning, Manassas, VA) with 10% FCS, 1% Pen/Strep, 621-101 in F12 media (Corning, Manassas, VA) with 10%FCS, 1% Pen/Strep. Para-Isothiocyanatobenzyl-desferrioxamine (*p*-SCN-Bn-DFO) was obtained from Macrocyclics (Dallas, TX) and used without further purification. Zirconium-89 was purchased from 3D Imaging, LLC (Maumelle, AR). Iodine-125 was purchased from Perkin Elmer. Human *holo*-transferrin was acquired from Sigma Aldrich.

**Flow Cytometry:** approximately  $1 \times 10^6$  cells per sample were lifted with Cellstripper (Corning, Manassas, VA), washed twice with PBS pH 7.4, and subsequently blocked with flow cytometry buffer (PBS, pH 7.4, 3% BSA). Anti-Human CD71 PE conjugated antibody (Invitrogen (eBioscience™, San Diego, CA) and PE Mouse anti-Rat CD71 antibody (BD Pharmigen™, San Jose, CA) was added to cells for 30 min on ice. Cells were extensively washed and fluorescence was quantified using a FACSCalibur (BD Biosciences). All flow cytometry data analysis was performed using FlowJo software FlowJo LLC (Ashland, Oregon).

**Bioconjugation chemistry:** Human *holo*-Tf (1.5 mg) was dissolved in 500  $\mu$ L of 0.1 M sodium bicarbonate buffer (pH 9.0). *p*-Bz-NCS-DFO (30 mM in DMSO, 4 eq.) was added to the Tf solution dropwise while mixing vigorously. The final concentration of DMSO was kept below 2% (v/v) to avoid any precipitation. The reaction was allowed to incubate for 30 min at 37°C, whereupon the reaction mixture was purified with a PD

G-25 (GE Healthcare, CA) column using an ammonium acetate mobile phase (0.2 M sodium acetate, pH 7.0). The Tf-DFO solution was aliquoted and stored at -20° C until time of use.

**Radiochemistry:** A solution of <sup>89</sup>Zr-oxalic acid (5mCi; 40 µl) was neutralized with 2M Na<sub>2</sub>CO<sub>3</sub> (18 µl). After 3 min, 0.30 ml of 0.5 M HEPES (pH 7.1–7.3) and 1.5 mg of DFO-Tf (pH = 7) were added into the reaction vial. After incubation for 60 min at 37°C, the reaction progress was monitored by iTLC using a 20 mM citric acid (pH 4.9–5.1) mobile phase. The decay corrected radiochemical yield was consistently > 95%. Radioiodination of Tf was performed in pre-coated iodination tubes (Pierce). 100 mg of transferrin was dispersed in 100 µL of PBS solution and added to the pre-coated iodination tubes. 0.5 mCi of iodine-125 was diluted with PBS up to 100 µL and added in the iodination tubes. After 15 min of reaction the solution was purified via PD G-25 (GE Healthcare, CA) column pre equilibrated with 10 mL of PBS solution. The purity was assessed *via* iTLC, and <sup>125</sup>I-Tf was always >98% pure.

**Cellular receptor binding assays:** Cells were seeded at a density of 4x10<sup>5</sup> cells per well in 12-well plates. On the day of the experiment, cells were subjected to a PBS wash followed by incubation for 30 min at 37°C, 5% CO<sub>2</sub> in PBS with <sup>125</sup>I-hTf (0.5 µCi). Thereafter the media was removed, and the residual unbound radiotracer was removed with two washes with ice cold PBS. The cell bound activity was harvested by lysis in 1 mL of 1M NaOH and collected. The unbound and cell-associated fractions were counted in a gamma counter and expressed as a percentage of the total activity added per well per cell number. Experiments were performed in quadruplicates, and the data are representative of at least two independent experiments.

**Small animal PET/CT:** All animal studies were conducted in compliance with Institutional Care and Use Committee at UCSF. Three to five-week-old intact male or female athymic nu/nu immunocompromised mice were purchased from Charles River. Nu/nu mice were inoculated with  $1.5 \times 10^6$  ELT3, 621-101, 105K, 97-1, RT4, tsc2 ang1 cells subcutaneously into one flank in a 1:1 mixture (v/v) of media (RPMI) and Matrigel (Corning). Xenografts were palpable within 14-40 days after injection. Tumor bearing mice (n=4 per treatment arm) received between 40 to 250  $\mu\text{Ci}$  of  $^{89}\text{Zr-Tf}$  in 100  $\mu\text{L}$  saline solution volume intravenously using a custom mouse tail vein catheter with a 28-gauge needle and a 100-150 mm long polyethylene microtubing. Approximately 200  $\mu\text{Ci}$  was injected for imaging studies and  $\sim 40$   $\mu\text{Ci}$  for biodistribution studies. The mice were imaged on a dedicated small animal PET/CT scanner (Inveon, Siemens Healthcare, Malvern, PA). Mice were imaged at 48 hours post injection. Animals were scanned for 40 minutes for PET, and the CT acquisition was 10 minutes. The co-registration between PET and CT images was obtained using the rigid transformation matrix from the manufacturer-provided scanner calibration procedure since the geometry between PET and CT remained constant for each of PET/CT scans using the combined PET/CT scanner. Animals were anesthetized with gas isoflurane at 2% concentration mixed with medical grade oxygen. The photon attenuation correction was performed for PET reconstruction using the co-registered CT-based attenuation map to ensure the quantitative accuracy of the reconstructed PET data.

**Autoradiography and Histology:** Tissues from euthanized animals were excised, submerged in Tissue-Plus OCT compound (Scigen, Gardena, CA), and frozen on dry ice. A series of 10  $\mu\text{m}$  tissue sections were cut and placed in a film cassette beneath a



phosphor-imaging plate for 48–72 h at  $-20\text{ }^{\circ}\text{C}$  (BASMS-2325; Fujifilm, Tokyo, Japan), which was then read on a Typhoon 7000IP plate reader (GE Healthcare, Chicago, IL) at  $25\text{ }\mu\text{m}$  pixel resolution. Several sequential sections were submitted to the Molecular Cytology Core Facility at UPenn for hematoxylin and eosin staining. A Zeiss Axioplan2 fluorescence microscope connected to a CCD camera and equipped with a motorized stage (Prior Scientific Instruments, Rockland, MA) was used to acquire microscopic images. MetaMorph software (Molecular Devices, Sunnyvale, CA) was used to control the microscope as well as to generate a montage of the entire tumor from the captured image frames. Image analysis was performed with ImageJ (<https://imagej.nih.gov/ij/>).

**Biodistribution studies:** Biodistribution studies were conducted to evaluate the uptake of in  $^{89}\text{Zr}$ -hTf mice bearing subcutaneous tumors. At a dedicated time after radiotracer injection, animals were euthanized by cervical dislocation, and blood or tissues were removed, weighed and counted on a gamma for accumulation of  $^{89}\text{Zr}$ -radioactivity. The mass of  $^{89}\text{Zr}$ -Tf formulation injected into each animal was measure and used to determine the total number of counts per minute by comparison to a standard syringe of known activity and mass. The data were background- and decay-corrected and the tissue uptake was expressed in units of percentage injected dose per gram of dry tissue (%ID/g).

**Statistical Analysis:** Data were analyzed using the unpaired, two-tailed Student's t-test using PRISM software. Differences at the 95% confidence level ( $P < 0.05$ ) were considered to be statistically significant.

## Figures:

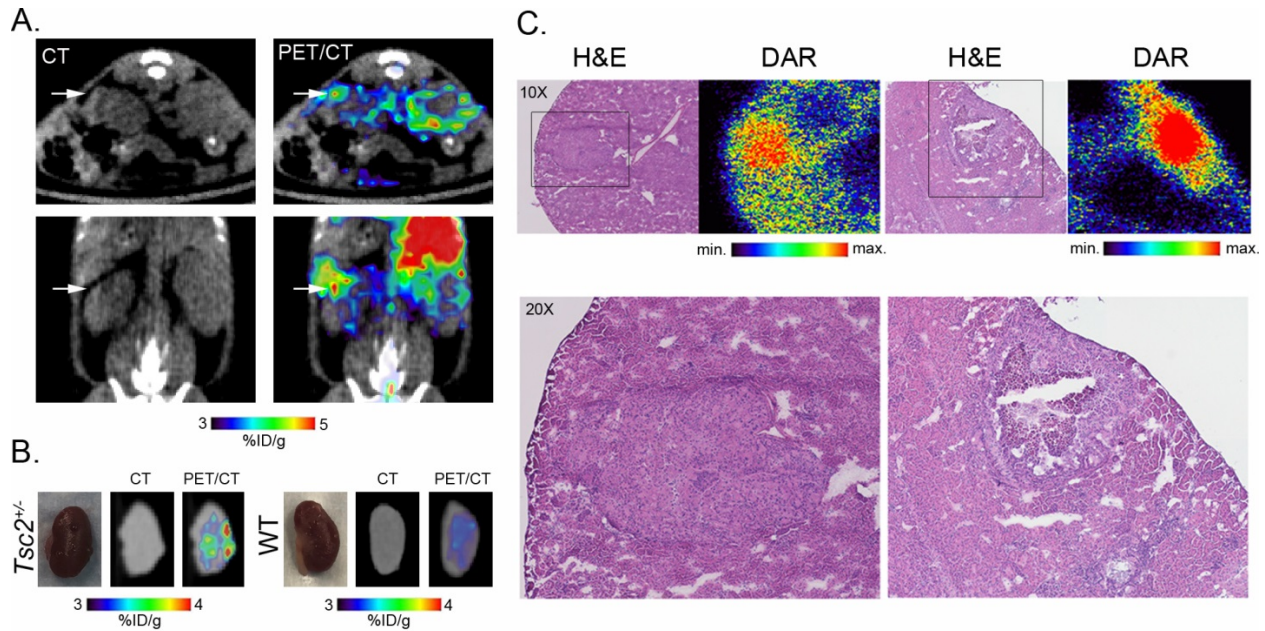


**Figure 1. <sup>89</sup>Zr-Tf detects spontaneous benign renal cystadenomas arising in A/J *Tsc2*<sup>+/-</sup> mice.** **A.** CT and PET/CT images showing the biodistribution of <sup>89</sup>Zr-Tf 48 hours after injection in *Tsc2*<sup>+/-</sup> mice. Several regions of aberrant density on CT were observed without added contrast agent that co-aligned with foci of high <sup>89</sup>Zr-Tf uptake. One focus is highlighted with a white arrow. **B.** PET/CT of surgically excised transgenic kidneys shows several regions of focal uptake of radiotracer significantly higher than the level of radiotracer observed in normal tissue. At right is shown a representative normal kidney from an immunocompetent mouse treated with an equivalent dose and uptake time of <sup>89</sup>Zr-Tf. **C.** Digital autoradiography (DAR) Showing the co-localization of <sup>89</sup>Zr-Tf with renal cystadenomas, detected on H&E. Two representative cystadenomas are shown at 20X magnification.

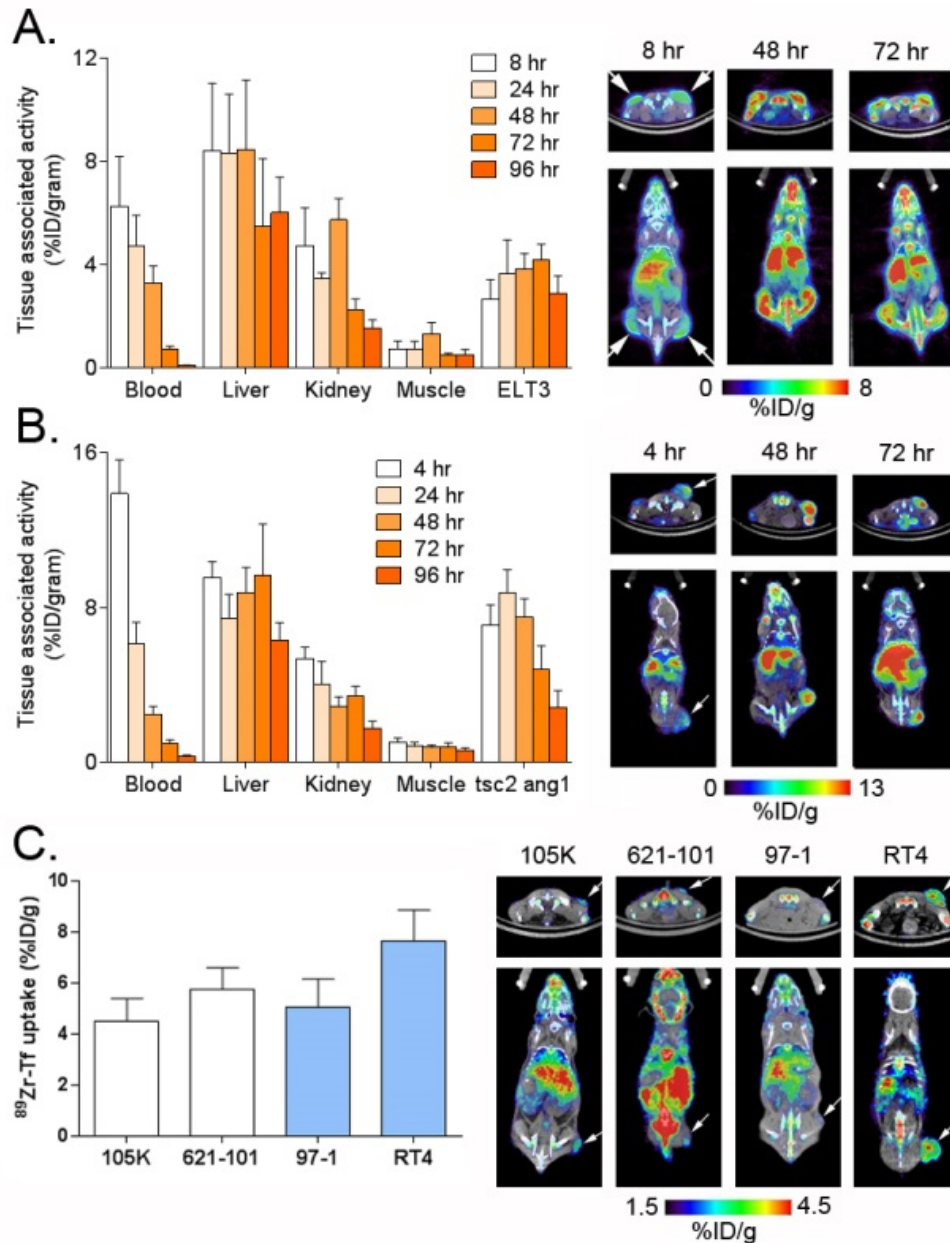


**Figure 2. Multiple cell line models harboring inactivating mutations in TSC1 or TSC2 are highly avid for  $^{89}\text{Zr}$ -Tf.** **A.** At left are shown data depicting the biodistribution of  $^{89}\text{Zr}$ -Tf in mice bearing subcutaneous ELT3 xenografts (a *Tsc2* mutant model of LAM). Radiotracer uptake peaked in the ELT3 tumors between 24-72 hours post injection, consistent with the pharmacology of  $^{89}\text{Zr}$ -Tf. Radiotracer uptake in representative normal tissues is also shown and has the expected degree of  $^{89}\text{Zr}$ -Tf accumulation. At right are shown representative coronal and transverse PET/CT images from a mouse in the cohort. The positions of the bilateral tumors are indicated with white arrows. **B.** At left are shown data depicting the biodistribution of  $^{89}\text{Zr}$ -Tf in mice bearing subcutaneous tsc2 ang1 xenografts (a *Tsc2* mutant model of AML). Radiotracer uptake peaked in the tsc2 ang1 tumors and exceeded blood pool levels at

24 hours post injection, Radiotracer uptake in representative normal tissues are also shown and have the expected degree of  $^{89}\text{Zr}$ -Tf accumulation. At right are shown representative coronal and transverse PET/CT images from a mouse in the cohort. The positions of the xenografts are indicated with a white arrow. **C.** At left are shown tumor uptake values for  $^{89}\text{Zr}$ -Tf acquired 48 hours post injection in mice bearing the indicated subcutaneous tumor. All tumor values exceeded blood pool, strongly suggesting uptake due to specific binding. White bars indicate cell line models harboring inactivating mutations in *Tsc2*, while blue bars highlight two human bladder cancer models with inactivating mutations in *Tsc1*. At right are shown representative PET/CT images. The position of the xenograft is highlighted with a white arrow.

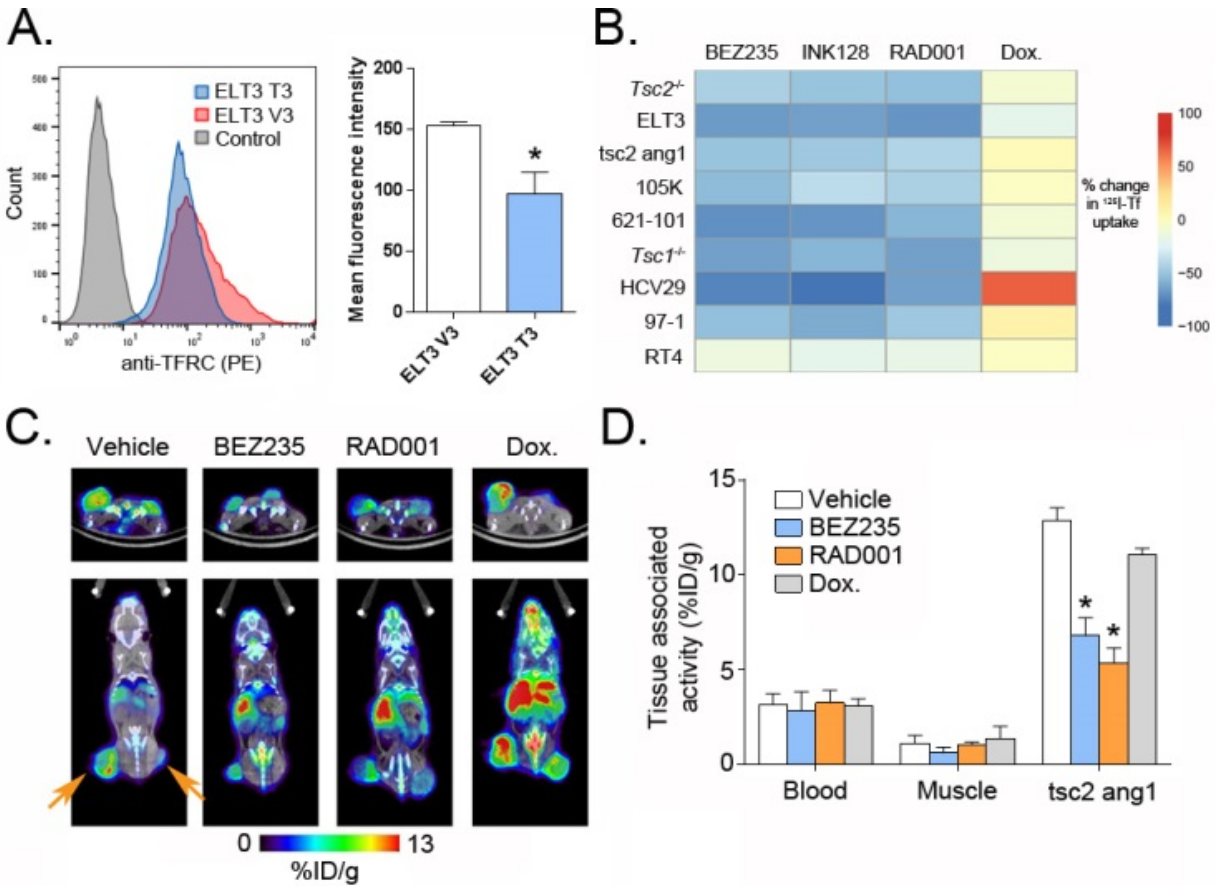


**Figure 3. TFRC expression and Tf uptake is mTORC1 dependent in LAM and TSC models.** **A.** Flow cytometry data showing that cell surface expression levels of TFRC are higher in *Tsc2* mutant ELT3 V3 cells compared to ELT T3, a subline with stable expression of wild type TSC2. Quantification of the mean fluorescence intensity from replicates shows the V3 cells have ~50% higher expression of cell surface TFRC. \* $P < 0.01$ . **B.** A heat map representing the percent change in <sup>125</sup>I-labeled Tf uptake in cells due to treatment with mechanistically discrete mTOR inhibitors (BEZ235, INK128, RAD001) or doxorubicin. Tf uptake is consistently repressed in *Tsc1* or *Tsc2* mutant cells, while a bioactive dose of doxorubicin does not alter Tf uptake (or mTORC1 activity). Data were acquired after 72 hours of drug exposure, and were normalized to cell number. **C.** Representative coronal and transverse PET/CT images showing the biodistribution of <sup>89</sup>Zr-Tf in mice bearing subcutaneous *tsc2 ang1* tumors after prior treatment with vehicle, BEZ235 (30 mg/kg) RAD001 (10 mg/kg) or doxorubicin (5 mg/kg). Mice were treated once daily for 5 days, and <sup>89</sup>Zr-Tf was injected on day 3 of the treatment course. ROI analysis at the tumor site showed a statistically significant decrease in <sup>89</sup>Zr-Tf uptake due to treatment with mTOR inhibitors compared to vehicle or doxorubicin treated mice. **D.** Tumor biodistribution data from the animal cohort treated as described in C. Blood and muscle values are shown as reference tissues not expected to be impacted by drug treatment. \* $P < 0.01$  compared to vehicle treated mice.

## References:

- Abe, N., Inoue, T., Galvez, T., Klein, L., and Meyer, T. 2008. Dissecting the role of PtdIns(4,5)P<sub>2</sub> in endocytosis and recycling of the transferrin receptor. *J Cell Sci* 121:1488-1494.
- Aggarwal, R., Behr, S.C., Paris, P.L., Truillet, C., Parker, M.F.L., Huynh, L.T., Wei, J., Hann, B., Youngren, J., Huang, J., et al. 2017. Real-Time Transferrin-Based PET Detects MYC-Positive Prostate Cancer. *Mol Cancer Res* 15:1221-1229.
- Arnold, R.T., and Myers, D.T. 2009. Visualization of renal angiomyolipoma on F-18 FDG PET/CT. *Clin Nucl Med* 34:539-540.
- Behr, S.C., Aggarwal, R., Seo, Y., Aparici, C.M., Chang, E., Gao, K.T., Tao, D.H., Small, E.J., and Evans, M.J. 2016. A Feasibility Study Showing [68Ga]Citrate PET Detects Prostate Cancer. *Mol Imaging Biol* 18:946-951.
- Chugani, H.T., Luat, A.F., Kumar, A., Govindan, R., Pawlik, K., and Asano, E. 2013. alpha-[11C]-Methyl-L-tryptophan--PET in 191 patients with tuberous sclerosis complex. *Neurology* 81:674-680.
- Crino, P.B., Nathanson, K.L., and Henske, E.P. 2006. The tuberous sclerosis complex. *N Engl J Med* 355:1345-1356.
- Fedi, M., Reutens, D.C., Andermann, F., Okazawa, H., Boling, W., White, C., Dubeau, F., Nakai, A., Gross, D.W., Andermann, E., et al. 2003. alpha-[11C]-Methyl-L-tryptophan PET identifies the epileptogenic tuber and correlates with interictal spike frequency. *Epilepsy Res* 52:203-213.
- Galvez, T., Teruel, M.N., Heo, W.D., Jones, J.T., Kim, M.L., Liou, J., Myers, J.W., and Meyer, T. 2007. siRNA screen of the human signaling proteome identifies the PtdIns(3,4,5)P<sub>3</sub>-mTOR signaling pathway as a primary regulator of transferrin uptake. *Genome Biol* 8:R142.

- Griffin, A. 2017. 18F-FDG PET/CT of Malignant Angiomyolipoma With Tumor Thrombus. *Clin Nucl Med* 42:628-629.
- Henske, E.P., Jozwiak, S., Kingswood, J.C., Sampson, J.R., and Thiele, E.A. 2016. Tuberous sclerosis complex. *Nat Rev Dis Primers* 2:16035.
- Henske, E.P., and McCormack, F.X. 2012. Lymphangiomyomatosis - a wolf in sheep's clothing. *J Clin Invest* 122:3807-3816.
- Ho, C.L., Chan, W.K., Chen, S., Leung, Y.L., and Cheng, T.K. 2010. Education and Imaging. Hepatobiliary and pancreatic: imaging for hepatic angiomyolipoma. *J Gastroenterol Hepatol* 25:1589.
- Huang, J., and Manning, B.D. 2008. The TSC1-TSC2 complex: a molecular switchboard controlling cell growth. *Biochem J* 412:179-190.
- Larson, S.M. 1978. Mechanisms of localization of gallium-67 in tumors. *Semin Nucl Med* 8:193-203.
- Lhommel, R., Annet, L., Bol, A., Gigot, J.F., Sempoux, C., Mathieu, I., Seret, M., and Lonneux, M. 2005. PET scan with 11C-acetate for the imaging of liver masses: report of a false positive case. *Eur J Nucl Med Mol Imaging* 32:629.
- Li, C., Lee, P.S., Sun, Y., Gu, X., Zhang, E., Guo, Y., Wu, C.L., Auricchio, N., Priolo, C., Li, J., et al. 2014. Estradiol and mTORC2 cooperate to enhance prostaglandin biosynthesis and tumorigenesis in TSC2-deficient LAM cells. *J Exp Med* 211:15-28.
- Lin, C.Y., Chen, H.Y., Ding, H.J., Yen, K.Y., and Kao, C.H. 2013. FDG PET or PET/CT in evaluation of renal angiomyolipoma. *Korean J Radiol* 14:337-342.
- Mari Aparici, C., Behr, S.C., Seo, Y., Kelley, R.K., Corvera, C., Gao, K.T., Aggarwal, R., and Evans, M.J. 2017. Imaging Hepatocellular Carcinoma With (68)Ga-Citrate PET: First Clinical Experience. *Mol Imaging* 16:1536012117723256.
- Nijmeh, J., El-Chemaly, S., and Henske, E.P. 2018. Emerging biomarkers of lymphangiomyomatosis. *Expert Rev Respir Med* 12:95-102.

- Onda, H., Lueck, A., Marks, P.W., Warren, H.B., and Kwiatkowski, D.J. 1999. Tsc2(+/-) mice develop tumors in multiple sites that express gelsolin and are influenced by genetic background. *J Clin Invest* 104:687-695.
- Pandit, N., and Yeung, H.W. 2001. F-18 FDG uptake in pulmonary lymphangioleiomyomatosis. *Clin Nucl Med* 26:1050-1051.
- Truillet, C., Cunningham, J.T., Parker, M.F.L., Huynh, L.T., Conn, C.S., Ruggero, D., Lewis, J.S., and Evans, M.J. 2017. Noninvasive Measurement of mTORC1 Signaling with 89Zr-Transferrin. *Clin Cancer Res* 23:3045-3052.
- Wu, J.Y., Peters, J.M., Goyal, M., Krueger, D., Sahin, M., Northrup, H., Au, K.S., Cutter, G., and Bebin, E.M. 2016. Clinical Electroencephalographic Biomarker for Impending Epilepsy in Asymptomatic Tuberous Sclerosis Complex Infants. *Pediatr Neurol* 54:29-34.
- Young, L.R., Franz, D.N., Nagarkatte, P., Fletcher, C.D.M., Wikenheiser-Brokamp, K.A., Galsky, M.D., Corbridge, T.C., Lam, A.P., Gelfand, M.J., and McCormack, F.X. 2009. Utility of [18F]2-fluoro-2-deoxyglucose-PET in sporadic and tuberous sclerosis-associated lymphangioleiomyomatosis. *Chest* 136:926-933.




**Publishing Agreement**

*It is the policy of the University to encourage the distribution of all theses, dissertations, and manuscripts. Copies of all UCSF theses, dissertations, and manuscripts will be routed to the library via the Graduate Division. The library will make all theses, dissertations, and manuscripts accessible to the public and will preserve these to the best of their abilities, in perpetuity.*

***Please sign the following statement:***

*I hereby grant permission to the Graduate Division of the University of California, San Francisco to release copies of my thesis, dissertation, or manuscript to the Campus Library to provide access and preservation, in whole or in part, in perpetuity.*

  
\_\_\_\_\_  
Author Signature

9/5/2018  
\_\_\_\_\_  
Date